applied optics

Tunable subwavelength terahertz plasmon-induced transparency in the InSb slot waveguide side-coupled with two stub resonators

HUAIQING LIU,[1,2] GUOBIN REN,[1,2,*] YIXIAO GAO,[1,2] YUDONG LIAN,[1,2] YANG QI,[1,2] AND SHUISHENG JIAN[1,2]

[1]Key Lab of All Optical Network & Advanced Telecommunication Network of EMC, Beijing Jiaotong University, Beijing 100044, China
[2]Institute of Lightwave Technology, Beijing Jiaotong University, Beijing 100044, China
*Corresponding author: gbren@bjtu.edu.cn

Received 23 January 2015; revised 18 March 2015; accepted 19 March 2015; posted 25 March 2015 (Doc. ID 232565); published 21 April 2015

We numerically investigated the realization of electromagnetically induced transparency (EIT) at the terahertz (THz) region in an InSb slot waveguide side-coupled with two stub resonators. The mechanism of the EIT phenomenon is theoretically analyzed and numerically studied by using coupled mode theory and the finite element method, respectively, and the theoretical results are in good agreement with the simulation results. The simulation results reveal that the EIT-like response is strongly dependent on the coupling separation between the two stub resonators, and we derived the best separation between the two stub resonators to get the most obvious EIT-like spectra. More importantly, the central wavelength of the EIT-like spectra can be actively controlled by tuning the temperature. This plasmonic waveguide system may have potential applications for ultracompact THz integrated circuits, such as thermo-tunable filters, THz switching, slow-light components, and THz sensitive sensors.

OCIS codes: (250.5403) Plasmonics; (040.2235) Far infrared or terahertz; (130.0130) Integrated optics; (240.6680) Surface plasmons.

http://dx.doi.org/10.1364/AO.54.003918

1. INTRODUCTION

Electromagnetically induced transparency (EIT) is a special and counterintuitive phenomenon that occurs in atomic systems due to the quantum destructive interference between the excitation pathways to the atomic upper level [1,2]. EIT is useful for many applications, such as bandpass filters, ultrafast switching, slow-light propagation, electro-optic modulators, transfer of quantum correlation, and nonlinear optical processes [3–11]. However, there are several specific and strict restrictions on the realization of the original EIT (based on the quantum interference of atomic resonances), making the experimental realization of it rather challenging. Recently, a number of classical configurations have been suggested for the realization of EIT-like transmission under less demanding experimental conditions, such as coupled dielectric resonators, metamaterial-induced transparency [12] and phase-coupled plasmon-induced transparency [13–16], detuned electrical dipoles [17], split-ring resonators [18], arrays of metallic nanoparticles [19], and plasmonic-waveguide systems [20,21]. Among these methods, plasmonic analogs of EIT in metallic nanostructures have attracted much attention in recent years. Compared to EIT in atomic media, plasmon-induced transparency can be operated at room temperature, and it has wide bandwidth and is easy to integrate [22].

Plasmonic devices, based on surface plasmon-polaritons (SPPs) propagating at the metal–dielectric interface, are regarded as the most promising candidates for the realization of highly integrated optical circuits due to significant overcoming of classical diffraction and manipulation of light at subwavelength scale [23]. Most of the efforts in plasmonic devices have been concentrated on optical and near-infrared frequencies [24–27]. Terahertz (THz) technology is now drawing extensive attention because of its potential applications in biochemical sensing, spectroscopy, and high-speed communication. With the rapid development of THz sources [28,29] and detectors [30], there is a high demand for THz components, such as waveguides, polarizers, filters, and collimators. So it is necessary to make efforts to study THz plasmonic devices, and there is an urgent need to explore new material that can support THz SPP waves. Some semiconductors have permittivity at the THz range close to that of metal at the optical range. InSb, whose permittivity can be modified by varying temperature [31,32],

has been proposed for designing THz plasmonic devices [33–35], which is a promising candidate for THz plasmonic devices, especially for THz sensors.

In this paper, the realization of EIT-like phenomena at the THz region in an InSb slot waveguide side-coupled with two stub resonators is theoretically analyzed and numerically studied by using coupled mode theory (CMT) and the finite element method (FEM), respectively. It is found that the EIT-like response is strongly dependent on the coupling distance between the two stub resonators, and we derived the best separation between the two stub resonators to get the most obvious EIT-like spectra. In addition, the central wavelength of the EIT-like response spectra can be actively controlled by tuning the temperature. The proposed structure may have great potential applications for ultracompact THz integrated circuits, such as thermo-tunable filters, THz switching, slow-light components, and THz sensitive sensors.

2. PLASMONIC SYSTEM AND MATERIAL PROPERTIES

Figure 1 shows an InSb slot waveguide that consists of a bus waveguide side-coupled with two stub resonators. The width of the slit and the two stub resonators is set as $w = 50$ μm (unchanged throughout this paper), the length of the two stub resonators is assumed as $L_1 = 300$ μm and $L_2 = 340$ μm, respectively, and the separation between the two stub resonators is d, which has much influence on the transmission spectra of our structure and will be discussed in detail in Section 4. The dispersion relation of the fundamental SPP mode in the InSb slot waveguide is given by [31]

$$\tanh\left(\sqrt{n_{\text{eff}}^2 - \varepsilon_d}\, k_0 w/2\right) = \frac{-\varepsilon_d \sqrt{n_{\text{eff}}^2 - \varepsilon_{\text{InSb}}(\omega)}}{\varepsilon_{\text{InSb}}(\omega)\sqrt{n_{\text{eff}}^2 - \varepsilon_d}}, \quad (1)$$

where n_{eff} is the effective refractive index of the SPP wave in the waveguide, $k_0 = 2\pi/\lambda_0$ is the free-space wave vector, $\beta = k_0 n_{\text{eff}}$, and λ_0 is the wavelength of the incident source. The insulator in the dielectric core is set as air, with permittivity $\varepsilon_d = 1$, and w and ω are the width of the air slit and the angular frequency of the incident light, respectively.

The permittivity of InSb can be approximately given by the simple Drude model approximation [36]:

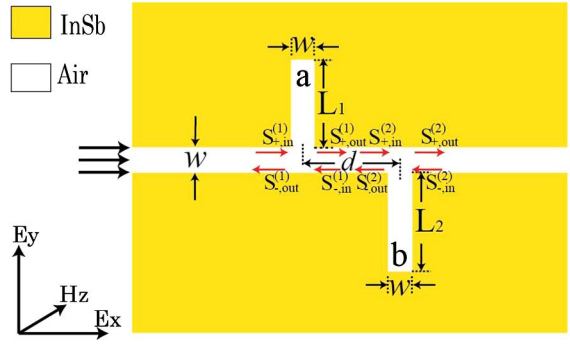

Fig. 1. Schematic diagram of our plasmonic system with an InSb slot waveguide side-coupled with two stub resonators. The geometric parameters are set as $w = 50$ μm, $L_1 = 300$ μm, and $L_2 = 340$ μm.

$$\varepsilon(\omega) = \varepsilon_\infty - \frac{\omega_p^2}{\omega^2 + i\gamma\omega}, \quad (2)$$

where ε_∞ represents the high-frequency permittivity, ω is the angular frequency, and γ is the damping constant. The plasma frequency $\omega_p = \sqrt{Ne^2/\varepsilon_0 m^*}$ depends on the intrinsic carrier density N, the electronic charge e, the vacuum permittivity ε_0, and the effective mass m^* of free carriers. One of the great differences between InSb and Ag is that the plasma frequency ω_p of InSb increases exponentially with the increase of temperature. The intrinsic carrier density N (in m^{-3}) of InSb obeys the relationship [37]

$$N = 5.76 \times 10^{20} T^{1.5} \exp(-0.26/2k_B T), \quad (3)$$

where k_B is the Boltzmann constant and T is the temperature in kelvin. It should be noted that the damping constant γ of InSb is proportional to the electron mobility μ as $\gamma = em^*/\mu$, which in turn depends on the temperature. Thus, while changing the temperature, γ will change as well and then it will influence the absorption property of InSb. However, when the temperature ranges from 160 to 350 K within the frequency regime from 0.1 to 2.2 THz, the electron mobility μ changes slightly. Consequently, the damping constant γ can be seen as a constant, which is consistent with the experimental report [38]. For InSb $\varepsilon_\infty = 15.6$, $m^* = 0.015m_e$ (m_e is the mass of electron), and $\gamma = 0.1\pi$ THz [39]. Figures 2(a) and 2(b) show the dependence of the real part and the imaginary part, respectively, of the effective refractive index of the InSb slot as a function of frequency at different temperatures with the width of the slot waveguide and the stub resonators kept as $w = 50$ μm. As shown in Fig. 2, we can see that the effective refractive index of InSb is affected by the variation of the temperature at THz region. Therefore, tunable plasmonic THz devices based on InSb material by tuning temperature seem interesting and promising.

3. ANALYTICAL MODEL AND THEORETICAL ANALYSIS

In this section, we focus on the comparison between the theoretical analysis results and the simulation results. The temperature is set as 280 K, unchanged throughout this part. The cross-section schematic diagram of our plasmonic systems is shown in Fig. 1. When a transverse-magnetic (TM) wave is injected and coupled into the bus waveguide, an SPP wave forms on the metallic interfaces and is confined in the waveguide. As the SPP wave passes through the coupled aperture, the energy can be nearly totally coupled into the stub resonator on the condition that the frequency of the incident source reaches the resonance frequency of the stub resonator. A single stub transmission spectrum exhibits a dip at the resonance frequency due to the destructive interference between the incident wave and escaped power from the resonator [as shown in Fig. 3(a)]. The dynamic transmission features can be investigated by the temporal CMT [40]. The normalized energy amplitudes a_N ($N = 1, 2$) of the Nth stub resonator can be described as

$$\frac{da_1}{dt} = (-j\omega_1 - \kappa_{o,1} - \kappa_{e,1})a_1 + e^{j\theta}\sqrt{\kappa_{e,1}}S_{+,\text{in}}^{(1)} + e^{j\theta}\sqrt{\kappa_{e,1}}S_{-,\text{in}}^{(1)}, \quad (4a)$$

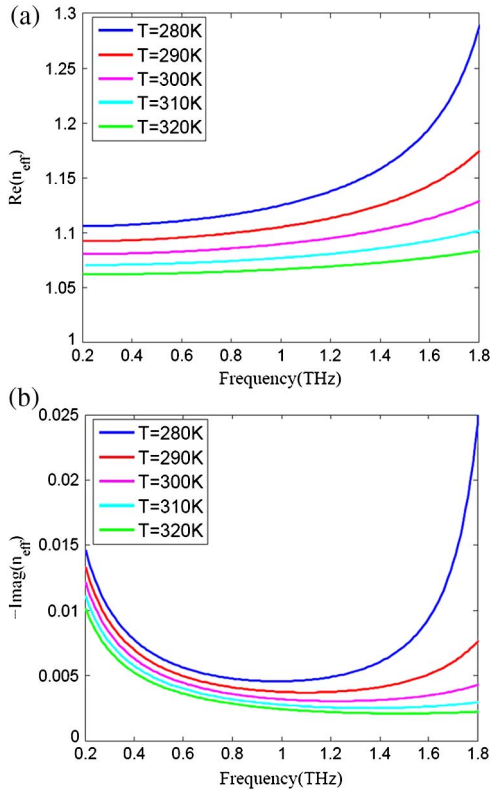

Fig. 2. (a) Real part of the effective refractive index of InSb slot waveguide as a function of frequency for different temperatures. (b) Imaginary part of the effective index of InSb slot waveguide versus frequency for different temperatures. The width of the slit is set as 50 μm in both figures.

$$\frac{da_2}{dt} = (-j\omega_2 - \kappa_{o,2} - \kappa_{e,2})a_2 + e^{j\theta}\sqrt{\kappa_{e,2}}S^{(2)}_{+,\text{in}} + e^{j\theta}\sqrt{\kappa_{e,2}}S^{(2)}_{-,\text{in}}, \tag{4b}$$

where ω_N $(N = 1, 2)$ represents the resonance frequency of the Nth stub resonator, $\kappa_{o,N}$ is the decay rate of the field due to internal loss in the Nth cavity, and $\kappa_{e,N}$ is the decay rate due to the energy escape into the bus waveguide. The decay rates satisfy the relationships $k_{o,N} = \omega_N/(2Q_{o,N})$, $k_{e,N} = \omega_N/(2Q_{e,N})$, where $Q_{o,N}$ and $Q_{e,N}$ stand for the intrinsic and coupling quality factors of the Nth resonator, respectively. θ is the phase of the coupling coefficient. The amplitudes of the incoming and outgoing waves in the bus waveguide are depicted by $S^N_{p,\text{in}}$ and $S^N_{p,\text{out}}$ $(N = 1, 2)$. The subscript $p = \pm$represents the two propagating directions of the waveguide modes, as shown in Fig. 1. With the conservation of energy, the outgoing waves of the cavities can be expressed as

$$\begin{aligned} S^{(1)}_{+,\text{out}} &= S^{(1)}_{+,\text{in}} - e^{-j\theta}\sqrt{\kappa_{e,1}}a_1, \\ S^{(2)}_{+,\text{out}} &= S^{(2)}_{+,\text{in}} - e^{-j\theta}\sqrt{\kappa_{e,2}}a_2, \end{aligned} \tag{5a}$$

$$\begin{aligned} S^{(2)}_{-,\text{out}} &= S^{(2)}_{-,\text{in}} - e^{-j\theta}\sqrt{\kappa_{e,2}}a_2, \\ S^{(1)}_{-,\text{out}} &= S^{(1)}_{-,\text{in}} - e^{-j\theta}\sqrt{\kappa_{e,1}}a_1. \end{aligned} \tag{5b}$$

In the linear system, since the input frequency is ω, the field always oscillates as $e^{-j\omega t}$, and $da_N/dt = -j\omega a_N$. The relationship between incoming and outgoing waves of the Nth stub resonator can be expressed as

$$\begin{aligned} S^{(N)}_{-,\text{in}} &= \frac{k_{e,N}}{j(\omega_N - \omega) + k_{o,N}} S^{(N)}_{+,\text{in}} \\ &\quad + \frac{j(\omega_N - \omega) + k_{o,N} + k_{e,N}}{j(\omega_N - \omega) + k_{o,N}} S^{(N)}_{-,\text{out}}, \end{aligned} \tag{6a}$$

$$\begin{aligned} S^{(N)}_{+,\text{out}} &= \frac{j(\omega_N - \omega) + k_{o,N} - k_{e,N}}{j(\omega_N - \omega) + k_{o,N}} S^{(N)}_{+,\text{in}} \\ &\quad - \frac{k_{e,N}}{j(\omega_N - \omega) + k_{o,N}} S^{(N)}_{-,\text{out}}. \end{aligned} \tag{6b}$$

The propagation waves in the waveguide should satisfy the relationship $S^{(1)}_{-,\text{in}} = S^{(2)}_{-,\text{out}}e^{j\varphi}$, and $S^{(2)}_{+,\text{in}} = S^{(1)}_{+,\text{out}}e^{j\varphi}$. Here, $\varphi = 2\pi\,\text{Re}(n_{\text{eff}})d/\lambda_0$ is the phase difference between the two stub resonators. λ_0 is the incident wavelength. n_{eff} is the effective refractive index of the SPP mode, which can be achieved from Eq. (1). The transmission and the reflection coefficients of the plasmonic system with a bus waveguide side-coupled to a single stub resonator are derived as

$$\begin{aligned} t_N(\omega) &= \frac{j(\omega_N - \omega) + k_{o,N}}{j(\omega_N - \omega) + k_{o,N} + k_{e,N}}, \\ r_N(\omega) &= -\frac{k_{e,N}}{j(\omega_N - \omega) + k_{o,N} + k_{e,N}}. \end{aligned} \tag{7}$$

When the incident source is only input from the left port $(S^{(2)}_{-,\text{in}} = 0)$, the line shape of the transmission can be written as

$$T = \left|\frac{S^{(2)}_{+,\text{out}}}{S^{(1)}_{+,\text{in}}}\right|^2 = \left|\frac{t_1 t_2}{1 - r_1 r_2 e^{j2\varphi}}\right|^2. \tag{8}$$

The above equation is a typical form of the transmission spectrum of a Fabry–Perot resonator with two frequency-dependent mirrors. Thus, the physical mechanism of the spectra response can be attributed to the Fabry–Perot oscillation. $t_{1,2}$ and $r_{1,2}$ are the frequency-dependent transmission and reflection coefficients of resonators a and b. In this paper, Comsol Multiphysics based on the FEM was utilized to investigate the transmission properties of our plasmonic system. The transmission spectra of our plasmonic system with a bus waveguide side-coupled with two stub resonators obtained by FEM and CMT are shown in Fig. 3(b). From Fig. 3(b), we can clearly see that there is a transparent window between the two dips, which correspond to the resonance frequency of the two different stub resonators. And it is obvious that the simulation results are in good agreement with the theoretical analysis. Figures 3(c)–3(e) show the contour profiles of $|H_z|$ of the proposed structure at different frequencies. It is obvious that the light was prevented from passing through this structure at the frequencies of 0.95 and 1.05 THz; however, it can pass through our structure at the frequency of 1 THz.

4. DEPENDENCE OF THE EIT-LIKE TRANSMISSION SPECTRA ON THE COUPLING DISTANCE BETWEEN THE TWO STUB RESONATORS

In this section, we investigate the influence of the coupling distance between the two stub resonators on the EIT-like

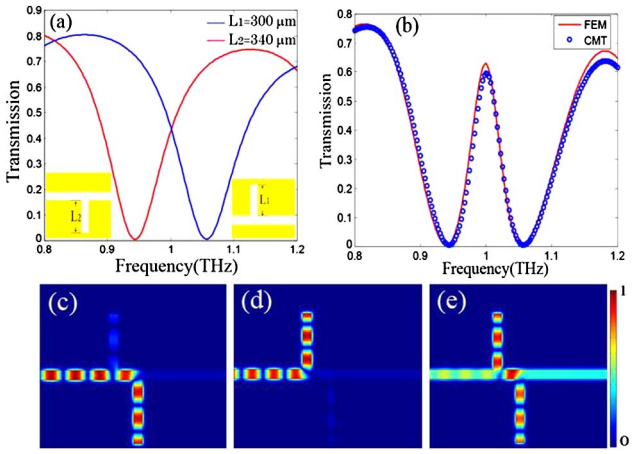

Fig. 3. (a) Transmission spectra for a single stub resonator coupled to a bus waveguide. (b) Simulation results and CMT results for combined two stub resonators side-coupled with a bus waveguide with $L_1 = 300$ μm and $L_2 = 340$ μm, respectively. $w = 50$ μm, and the coupling distance between the two stub resonators d is 134 μm. The contour profiles of $|H_z|$ of the proposed structure correspond to (b) at different frequencies of (c) $f = 0.95$ THz, (d) $f = 1.05$ THz, and (e) $f = 1$ THz.

transmission spectra. The temperature is set as 280 K throughout this section. Here, we set $L_1 = 300$ μm and $L_2 = 340$ μm, and $w = 50$ μm. By changing d, the transmission spectra as a function of frequency for different d are plotted in Fig. 4. It is found that the EIT-like transmission spectra appear and vanish while changing the separation between the two stub resonators.

In order to investigate the influence of the coupling distance on the transmission spectra of our structure, we consider the phase difference between the two stub resonators. The phase difference between the two stub resonators can be written as $\varphi = d n_{\text{eff}} k_0 = 2d\,\text{Re}(n_{\text{eff}})\pi/\lambda_0$. From the Fabry–Perot model, the transmission will be enhanced if the Fabry–Perot resonant condition is satisfied. Defining $\Delta\phi$ to be the accumulated phase delay per round trip inside the FP resonator, one has $\Delta\phi = 2\varphi + \phi_1 + \phi_2$, where $\varphi = k_{\text{spp}} d = 2\pi\,\text{Re}(n_{\text{eff}})d/\lambda_0$ is the phase difference between the two mirrors, λ_0 is the wavelength of the incident wave, n_{eff} is the effective refractive index of the SPP mode in the waveguide, and d is the distance between the two mirrors. ϕ_1 and ϕ_2 are the phase shifts caused by reflection of mirror a and mirror b, respectively. The pronounced EIT-like transparency peak appears nearly at the middle of the two dips when the phase delay satisfies $\Delta\phi = 2n\pi (n = 0, 1, 2\ldots)$ [41], which is a constructive interference condition in the FP resonator. Combining this equation and $\varphi = 2d\,\text{Re}(n_{\text{eff}})\pi/\lambda_0$, we can get the best coupling distance to get the most obvious EIT-like spectra as

$$d = \frac{\lambda_0}{2n_{\text{eff}}}[n - (\phi_1 + \phi_2)/(2\pi)], \qquad (n = 0, 1, 2\ldots). \quad \textbf{(9)}$$

The phase shifts ϕ_1 and ϕ_2 can also be calculated numerically [42]. As the terms of $(\phi_1 + \phi_2)/(2\pi)$ are very small [43,44], Eq. (9) can be approximated as

$$d = \frac{n\lambda_0}{2\,\text{Re}(n_{\text{eff}})}, \qquad (n = 0, 1, 2\ldots). \quad \textbf{(10)}$$

It worth noting that the transmission spectra as a function of φ have the same value at the phase difference $\Delta\varphi = n\pi$ $(n = 1, 2, 3\ldots)$, so according to Eq. (10), the distance difference of the adjacent period is

$$\Delta d = \lambda_0/(2\,\text{Re}(n_{\text{eff}})). \quad \textbf{(11)}$$

The dispersion relationship for the SPP mode of the proposed structure with slit width of 50 μm and temperature of 280 K is plotted in Fig. 5(a). In Eq. (10), we take $n = 1$ as an example to analyze the influence of d on the transmission spectra; when $n = 1$, Eq. (10) can be written as $d = \lambda_0/(2\,\text{Re}(n_{\text{eff}}))$, and according to this equation, the best separation between the two stub resonators with the most obvious EIT-like transmission spectra for various frequencies is plotted in Fig. 5(b). Figure 5(c) shows the simulation results of the transmission spectra as a function of the frequency of the incident wave and the separation between the two stub resonators; the four dots of light in the blue region represent the peaks of the transparent window corresponding to $n = 0$, 1, 2, 3 in Eq. (10), respectively. For example, when $n = 1$, according to the simulation results in Fig. 5(c), the separation with the most obvious EIT-like spectra is about 134 μm, which is in agreement with the theoretical analysis results as shown in Fig. 5(b) (about 137 μm). The slight difference between the theoretical analysis results and the FEM method is caused by neglecting the phase shifts caused by reflection of the two mirrors. From Fig. 5(c), it is found that the transparency peak between the two dips appears periodically with different separations between the two stub resonators, and the period is about 134 μm, which is in good agreement with the theoretical analysis results obtained from Eq. (11). And at 1 THz, the transmission spectra of our structure versus the separation between the two stub resonators is plotted in Fig. 5(d); it is obvious that the transparency peak between the two dips appears periodically while changing the separation between the two stub resonators. So the most obvious EIT-like spectra can be achieved by manipulating the separation between the two stub resonators.

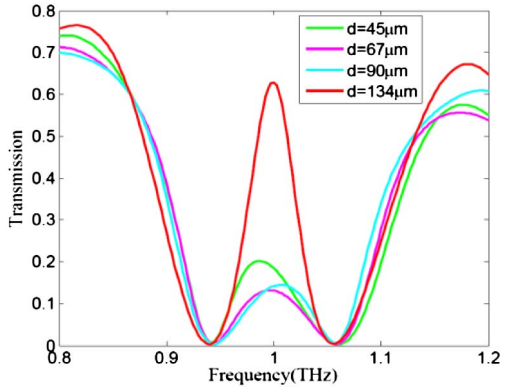

Fig. 4. Transmission spectra as a function of frequency for different separations between the two stub resonators with $w = 50$ μm, $L_1 = 300$ μm, and $L_2 = 340$ μm.

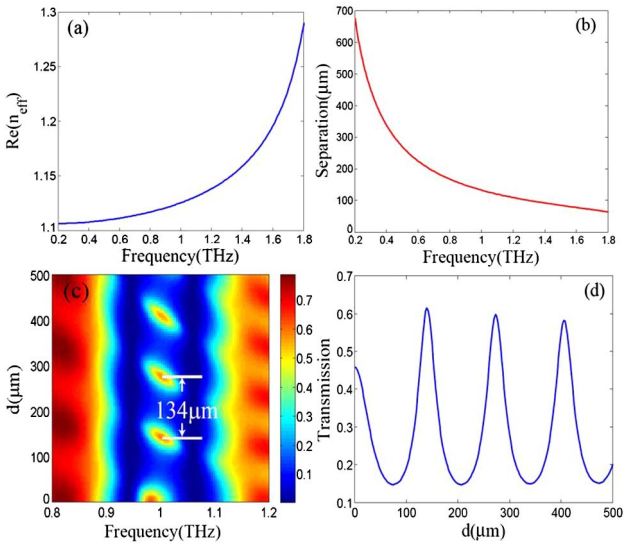

Fig. 5. (a) Real part of the effective refractive index of SPP mode with $w = 50$ μm. (b) Separations between the two stub resonators at different central frequencies corresponding to the most obvious EIT-like response. (c) Transmission spectra as a function of the frequency of the incident light and the separation between the two stub resonators. (d) Transmission spectra versus the separation between the two stub resonators at 1 THz.

5. THERMO-TUNABLE PROPERTIES OF THE EIT-LIKE TRANSMISSION SPECTRA IN OUR STRUCTURE

As mentioned in Section 2, the optical property of InSb is determined by temperature, based on which we can manipulate the transmission spectra of our structure by tuning the temperature. In this section, we investigate the influence of the temperature on the transmission of our structure. The geometric parameters except d throughout this section are set as $w = 50$ μm, $L_1 = 300$ μm, and $L_2 = 340$ μm. Figures 6(a) and 6(b) show the transmission spectra of the proposed structure as a function of frequency for different temperatures with $d = 134$ μm and $d = 0$ μm, respectively.

As shown in Fig. 6, it is obvious that EIT-like transmission spectra can be achieved both when $d = 134$ μm and when $d = 0$ μm, which correspond to $n = 1$ and $n = 0$ in Eq. (10), respectively. We can clearly see that the central wavelength of the EIT-like response spectra shifts to higher frequency while increasing the temperature. This phenomenon can be explained in this way: the dip of the transmission spectra of our structure with a single stub resonator [as shown in the inset of Fig. 3(a)] can be written as [31] $\lambda_m = 4n_{\text{eff}}L/(2m+1)$, where n_{eff} is the effective refractive index of the SPP mode, L is the length of the stub resonator, and positive integer m is the order of the resonance mode in the stub resonator. Since $f = c/\lambda$, the dip of the transmission spectra of the plasmonic system with a single stub resonator coupled to a bus waveguide can be expressed as

$$f_m = [(2m+1)]c/(4n_{\text{eff}}L). \quad (12)$$

According to Fig. 2(a), increasing temperature will result in a lower value of n_{eff}, and a lower n_{eff} will lead to a higher value

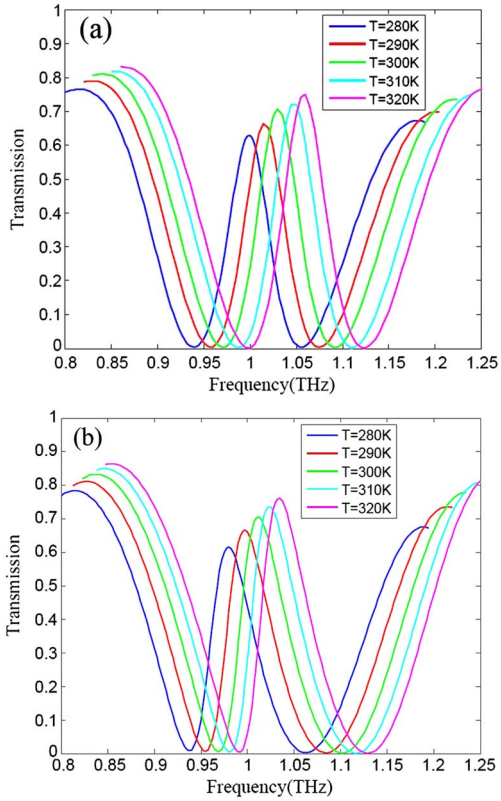

Fig. 6. Transmission spectra as a function of frequency for various temperatures ranging from 280 to 320 K with $w = 50$ μm, $L_1 = 300$ μm, and $L_2 = 340$ μm for (a) $d = 134$ μm and (b) $d = 0$ μm.

of f_m according to Eq. (12), so increasing temperature will shift the two resonance dips of the transmission spectra to a higher frequency, and the central frequency of the EIT-like response spectra will shift to a higher frequency as a result. It worth noting that the transmission peak moves to a higher value with the increase of temperature, and according to Fig. 2(b), increasing temperature will reduce the value of the imaginary part of the effective refractive index of the SPP mode in the proposed InSb slot waveguide, which is good for reducing the absorption loss in our structure, so a higher temperature will lead to a higher transmission peak of the EIT-like transparent window.

We have also investigated the sensitivity of the central frequency of the EIT-like transmission spectra on temperature. The central frequency of the EIT-like spectra as a function of temperature with $d = 134$ μm is shown in Fig. 7. It is found that the central frequency of the EIT-like transmission spectra is nearly linear to the temperature; the circular blue points are the simulation results, and the red line represents the linear fit of the simulation results. So we can easily manipulate the EIT-like transmission spectra by varying the temperature instead of changing the geometric parameters, which is good for practical applications of the proposed plasmonic system. In addition, as the central frequency of the EIT-like transmission spectra is sensitive to the change of temperature, and the sensitivity is about 1.425×10^{-3} THz/°C obtained from Fig. 7,

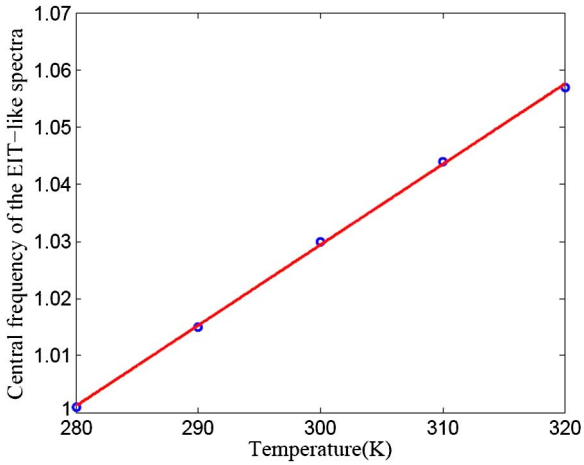

Fig. 7. Central frequency of the EIT-like transmission spectra as a function of temperature; the geometric parameters of the structure are the same as in Fig. 6(a).

corresponding to 427.5 nm/°C, so the proposed structure can also act as a good THz sensor.

6. CONCLUSION

In summary, we have numerically and theoretically investigated EIT-like transmission spectra at the THz region in a plasmonic system consisting of an InSb slot waveguide side-coupled with two stub resonators. The theoretical results obtained from CMT are in good agreement with the FEM simulations. The simulation results reveal that the transmission spectra depend on the separation between the two stub cavities, and the most obvious EIT-like spectra will emerge only if the accumulated phase delay per round trip in the FP resonator satisfies the constructive interference condition, based on which we derived the best separations to get the most obvious EIT-like spectra. In addition, thanks to the thermo-tunable properties of InSb, the central frequency of the EIT-like spectra can be tuned by varying the temperature. On the other hand, as the EIT-like spectra are sensitive to the change of the temperature (427.5 nm/°C), the proposed structure can also act as a good THz sensor. The proposed structure opens the possibility for future applications in highly integrated THz devices, such as thermo-tunable filters, THz switching, slow-light components, and THz sensors.

The National Natural Science Foundation of China (NSFC) (Grant Nos. 61178008 and 61275092).

REFERENCES

1. K. J. Boller, A. Imamolu, and S. Harris, "Observation of electromagnetically induced transparency," Phys. Rev. Lett. **66**, 2593–2596 (1991).
2. M. Fleischhauer, A. Imamoglu, and J. Marangos, "Electromagnetically induced transparency: optics in coherent media," Rev. Mod. Phys. **77**, 633–673 (2005).
3. R. W. Boyd and D. J. Gauthier, "Photonics: transparency on an optical chip," Nature **441**, 701–702 (2006).
4. R. D. Kekatpure, E. S. Barnard, and W. Cai, "Phase-coupled plasmon-induced transparency," Phys. Rev. Lett. **104**, 243902 (2010).
5. H. Lu, X. Liu, and G. Wang, "Tunable high-channel-count bandpass plasmonic filters based on an analogue of electromagnetically induced transparency," Nanotechnology **23**, 444003 (2012).
6. H. Lu, X. Liu, and D. Mao, "Plasmonic analog of electromagnetically induced transparency in multi-nanoresonator-coupled waveguide systems," Phys. Rev. A **85**, 053803 (2012).
7. Y. Zhang, K. Hayasaka, and K. Kasai, "Conditional transfer of quantum correlation in the intensity of twin beams," Phys. Rev. A **71**, 062341 (2005).
8. S. Harris and L. Hau, "Nonlinear optics at low light levels," Phys. Rev. Lett. **82**, 4611–4614 (1999).
9. Y. Cui and C. Zeng, "Optical bistability based on an analog of electromagnetically induced transparency in plasmonic waveguide-coupled resonators," Appl. Opt. **51**, 7482–7486 (2012).
10. G. Wang, H. Lu, and X. Liu, "Dispersionless slow light in MIM waveguide based on a plasmonic analogue of electromagnetically induced transparency," Opt. Express **20**, 20902–20907 (2012).
11. J. Chen, Z. Li, and X. Zhang, "Submicron bidirectional all-optical plasmonic switches," Sci. Rep. **3**, 1451 (2013).
12. F. Zhang, Q. Zhao, and C. Lan, "Magnetically coupled electromagnetically induced transparency analogy of dielectric metamaterial," Appl. Phys. Lett. **104**, 131907 (2014).
13. H. Lu, X. Liu, and D. Mao, "Induced transparency in nanoscale plasmonic resonator systems," Opt. Lett. **36**, 3233–3235 (2011).
14. G. Cao, H. Li, and S. Zhan, "Uniform theoretical description of plasmon-induced transparency in plasmonic stub waveguide," Opt. Lett. **39**, 216–219 (2014).
15. G. Cao, H. Li, and S. Zhan, "Formation and evolution mechanisms of plasmon-induced transparency in MDM waveguide with two stub resonators," Opt. Express **21**, 9198–9205 (2013).
16. C. Zeng, "Plasmonic spectral splitting in multi-resonator-coupled waveguide systems," Appl. Opt. **53**, 38–43 (2014).
17. Z. G. Dong, H. Liu, and M. X. Xu, "Plasmonically induced transparent magnetic resonance in a metallic metamaterial composed of asymmetric double bars," Opt. Express **18**, 18229–18234 (2010).
18. Y. Guo, L. Yan, and W. Pan, "Electromagnetically induced transparency (EIT)-like transmission in side-coupled complementary split-ring resonators," Opt. Express **20**, 24348–24355 (2012).
19. V. Yannopapas, E. Paspalakis, and N. Vitanov, "Electromagnetically induced transparency and slow light in an array of metallic nanoparticles," Phys. Rev. B **80**, 035104 (2009).
20. K. Wen, L. Yan, and W. Pan, "Electromagnetically induced transparency-like transmission in a compact side-coupled T-shaped resonator," J. Lightwave Technol. **32**, 1701–1707 (2014).
21. G. Cao, H. Li, and Y. Deng, "Plasmon-induced transparency in a single multimode stub resonator," Opt. Express **22**, 25215–25223 (2014).
22. S. Zhang, D. A. Genov, and Y. Wang, "Plasmon-induced transparency in metamaterials," Phys. Rev. Lett. **101**, 047401 (2008).
23. S. I. Bozhevolnyi, V. S. Volkov, and E. Devaux, "Channel plasmon subwavelength waveguide components including interferometers and ring resonators," Nature **440**, 508–511 (2006).
24. J. Chen, C. Wang, and R. Zhang, "Multiple plasmon-induced transparencies in coupled-resonator systems," Opt. Lett. **37**, 5133–5135 (2012).
25. K. Wen, Y. Hu, and L. Chen, "Single/multiple-mode-selection optical nanofilters based on end-coupled split-ring resonators," Appl. Opt. **53**, 4158–4163 (2014).
26. K. Wen, L. Yan, and W. Pan, "A four-port plasmonic quasi-circulator based on metal-insulator-metal waveguides," Opt. Express **20**, 28025–28032 (2012).
27. J. Chen, Z. Li, and J. Li, "Compact and high-resolution plasmonic wavelength demultiplexers based on Fano interference," Opt. Express **19**, 9976–9985 (2011).
28. M. A. Belkin, W. Qi Jie, and C. Pflugl, "High-temperature operation of terahertz quantum cascade laser sources," IEEE J. Sel. Top. Quantum Electron. **15**, 952–967 (2009).
29. G. Liang, H. Liang, and Y. Zhang, "Single-mode surface-emitting concentric-circular-grating terahertz quantum cascade lasers," Appl. Phys. Lett. **102**, 031119 (2013).

30. S. Komiyama, O. Astafiev, and V. V. Antonov, "A single-photon detector in the far-infrared range," Nature **403**, 405–407 (2000).
31. J. Tao, B. Hu, and X. Y. He, "Tunable subwavelength terahertz plasmonic stub waveguide filters," IEEE Trans. Nanotechnol. **12**, 1191–1197 (2013).
32. W. Li, D. Kuang, and F. Fan, "Subwavelength B-shaped metallic hole array terahertz filter with InSb bar as thermally tunable structure," Appl. Opt. **51**, 7098–7102 (2012).
33. L. Deng, J. Teng, and H. Liu, "Direct optical tuning of the terahertz plasmonic response of InSb subwavelength gratings," Adv. Opt. Mater. **1**, 128–132 (2013).
34. B. Hu, Q. J. Wang, and Y. Zhang, "Broadly tunable one-way terahertz plasmonic waveguide based on nonreciprocal surface magneto plasmons," Opt. Lett. **37**, 1895–1897 (2012).
35. J. GóMez Rivas, M. Kuttge, and H. Kurz, "Low-frequency active surface plasmon optics on semiconductors," Appl. Phys. Lett. **88**, 082106 (2006).
36. J. Sánchez-Gil and J. Rivas, "Thermal switching of the scattering coefficients of terahertz surface plasmon polaritons impinging on a finite array of subwavelength grooves on semiconductor surfaces," Phys. Rev. B **73**, 205410 (2006).
37. M. Oszwałldowski and M. Zimpel, "Temperature-dependence of intrinsic carrier concentration and density of states effective mass of heavy holes in InSb," J. Phys. Chem. Solids **49**, 1179–1185 (1988).
38. S. C. Howells and L. A. Schlie, "Transient terahertz reflection spectroscopy of undoped InSb from 0.1 to 1.1 THz," Appl. Phys. Lett. **69**, 550–552 (1996).
39. X. Dai, Y. Xiang, and S. Wen, "Thermally tunable and omnidirectional terahertz photonic bandgap in the one-dimensional photonic crystals containing semiconductor InSb," J. Appl. Phys. **109**, 053104 (2011).
40. C. Manolatou, M. J. Khan, and S. Fan, "Coupling of modes analysis of resonant channel add-drop filters," IEEE J. Quantum Electron. **35**, 1322–1331 (1999).
41. F. Hu, H. Yi, and Z. Zhou, "Wavelength demultiplexing structure based on arrayed plasmonic slot cavities," Opt. Lett. **36**, 1500–1502 (2011).
42. J. S. White, G. Veronis, and Z. Yu, "Extraordinary optical absorption through subwavelength slits," Opt. Lett. **34**, 686–688 (2009).
43. F. Hu, H. Yi, and Z. Zhou, "Band-pass plasmonic slot filter with band selection and spectrally splitting capabilities," Opt. Express **19**, 4848–4855 (2011).
44. Q. Zhang, X.-G. Huang, and X.-S. Lin, "A subwavelength coupler-type MIM optical filter," Opt. Express **17**, 7549–7555 (2009).